

Microfluidic Evolution-On-A-Chip Reveals New Mutations that Cause Antibiotic Resistance

Ahmed E. Zoheir, Georg P. Späth, Christof M. Niemeyer, and Kersten S. Rabe*

Microfluidic devices can mimic naturally occurring microenvironments and create microbial population heterogeneities ranging from planktonic cells to biofilm states. The exposure of such populations to spatially organized stress gradients can promote their adaptation into complex phenotypes, which are otherwise difficult to achieve with conventional experimental setups. Here a microfluidic chip that employs precise chemical gradients in consecutive microcompartments to perform microbial adaptive laboratory evolution (ALE), a key tool to study evolution in fundamental and applied contexts is described. In the chip developed here, microbial cells can be exposed to a defined profile of stressors such as antibiotics. By modulating this profile, stress adaptation in the chip through resistance or persistence can be specifically controlled. Importantly, chip-based ALE leads to the discovery of previously unknown mutations in *Escherichia coli* that confer resistance to nalidixic acid. The microfluidic device presented here can enhance the occurrence of mutations employing defined micro-environmental conditions to generate data to better understand the parameters that influence the mechanisms of antibiotic resistance.

1. Introduction

The ability of microorganisms to adapt to different physico-chemical environments is a key characteristic of life.^[1] This fundamental process can be harnessed to intentionally trigger living systems to gain novel traits or to enhance their inherited characteristics in a process termed adaptive laboratory evolution (ALE).^[2,3] ALE is an essential methodology to investigate fundamental questions ranging from the evolution of life and

its underlying mechanisms to the adaptation of microbial populations to their environments, such as the emergence of antibiotic resistance.^[4-7] Especially in biotechnological production, ALE has been employed to improve yields or to enhance the microorganism's tolerance to toxic conditions.^[2,3] Although ALE has many applications, it is simply based on the general principle of biological evolution, involving two interplaying processes: genetic variation and selection.^[4] Genetic mutations occur naturally during the DNA replication as spontaneous rare events,^[4,8] but their occurrence can be enhanced in response to stress or external factors.^[4,8] Some mutations enable the microorganism to grow better under normally inhibitory conditions. Selection of such advantageous traits is the goal of ALE.

Technically, the simplest ALE setup utilizes conventional cultivation equipment such as shake flasks for serially passaging

of batch cultures for prolonged time, with a stepwise increase of selection pressure.^[9] Such methods are very laborious and require culture manipulation on a daily basis for up to months. Therefore, liquid-handling robots,^[10] conventional bioreactors,^[11] as well as tailor-made cultivation devices^[12,13] have been employed to automate and reduce the hands-on time of ALE. Nevertheless, these techniques usually require expensive equipment and specially trained personnel, which hinders their widespread use in common microbiological laboratories.

It is relevant that the ALE techniques mentioned above mainly involve vigorous mixing of planktonic bacteria in a defined chemical environment, and therefore pay less attention to the role of other natural adaptive mechanisms. For example, microenvironments rich in spatial physico-chemical gradients are omnipresent in nature and often characterize the habitat of planktonic and biofilm populations.^[14,15] Since phenotypic heterogeneity as well as the formation of biofilm communities can also allow cells to adopt a sustainable lifestyle without genetic modification, the resulting stress persistence needs to be taken into account when optimizing ALE. To address this issue, advanced microtechnical solutions for ALE should also include 3D microenvironments as protected habitats that can favor population heterogeneity. Recent studies have emphasized the importance of concentration gradients and heterogenic microenvironments on the composition and adaptability of bacterial populations.^[16-19] The integration of spatial chemical gradients^[18] within meso and macroscopic ALE systems, however, is technically challenging.

Dr. A. E. Zoheir, G. P. Späth, Prof. C. M. Niemeyer, Dr. K. S. Rabe
Institute for Biological Interfaces 1 (IBG-1)
Karlsruhe Institute of Technology (KIT)
Hermann-von-Helmholtz-Platz 1, Eggenstein-Leopoldshafen 76344,
Germany
E-mail: kersten.rabe@kit.edu

Dr. A. E. Zoheir
Department of Genetics and Cytology
National Research Centre (NRC)
33 El Buhouth St., Cairo 12622, Egypt

 The ORCID identification number(s) for the author(s) of this article can be found under <https://doi.org/10.1002/sml.202007166>.

© 2021 The Authors. Small published by Wiley-VCH GmbH. This is an open access article under the terms of the Creative Commons Attribution-NonCommercial License, which permits use, distribution and reproduction in any medium, provided the original work is properly cited and is not used for commercial purposes.

DOI: 10.1002/sml.202007166

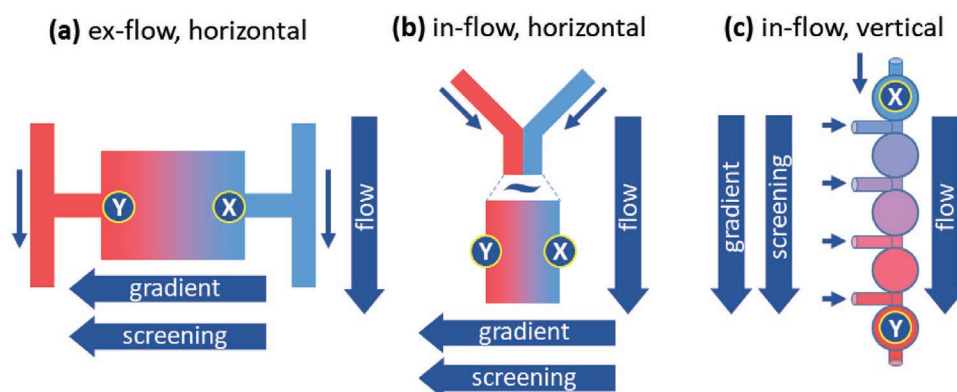


Figure 1. Concepts of gradient generation. The gradient chamber in which cultivation takes place can be located either outside or inside the flow, dubbed as a) ex-flow and b,c) in-flow gradients, respectively. In commonly used ex- and in-flow (a,b) systems, the direction of the gradient and screening are oriented horizontally to the flow direction, while in the herein applied design (c), they are vertical to the flow direction. While in areas with low stressor concentration (blue, minimum = X) the cells can grow well, in areas with high stress (red, maximum = Y) the screening and enrichment of mutants with increased fitness takes place.

Miniaturized fluidic chip systems are gaining a steadily growing impact on the analysis of microbial systems,^[20–24] and microfluidic devices with integrated spatial concentration gradients have been successfully used for toxicity testing^[25,26] and directed evolution.^[27,28] However, the ability to generate spatially defined gradients of stressors is still limited. Additionally, screening of the adapted mutants in these systems is not well optimized for robust, long-term ALE experiments, which often lead to clogging of the chip due to accumulated biomass and obstruction of the sensitive gradient-generating flow systems. Due to these obstacles, the majority of microbial studies in microfluidic gradients usually do not encompass cultivations for more than 2 days^[27,29–32] and may not be able to discover adaptations that often manifest themselves only after prolonged cultivation.^[7,33] To overcome these limitations and to enable long-term ALE experiments with efficient screening under unfavorable high stress conditions, we here describe a novel, robust, and user-friendly miniaturized ALE chip design that employs adjustable spatial stress profiles and an in-flow gradient while at the same time enabling efficient on-chip screening of the complete cell population.

2. Results and Discussion

2.1. Design Strategy

Commonly used microfluidic gradient structures for microbial studies can be classified according to where the cultivation chamber containing the gradient is located in relation to the flow. Therefore, one has to distinguish between ex-flow^[17,30,34] (Figure 1a) and in-flow^[29,35,36] (Figure 1b) gradients. In both systems the gradient is usually oriented horizontally to the flow direction (Figure 1a,b), thus screening and enrichment of the adapted mutants depends on cells moving from the low stress areas (Figure 1a,b, X) toward areas of high stressor concentration (Figure 1a,b, Y) either actively as motile cells or passively due to the increase in biomass. Bacterial motility is indeed controlled by chemotactic decisions that usually will avoid high-stress environments,^[28] thus impeding effective selection in

ALE. To solve this problem, many systems require special nutrients arrangements, such as low nutrients at low stress areas, and high nutrients at high stress areas, in order to attract motile cells via chemotaxis for screening at high stress, which can lead to a more complex and potentially error-prone design.^[28,37] For the in-flow approach (Figure 1b), the active cell movement will be additionally deflected by the orthogonal flow forces of the medium in the chip. Therefore, in these gradient approaches adapted cells potentially never reach the high-stress areas of the chip where the selection can occur (Figure 1a,b, Y).^[28]

To address this shortcoming, the current work uses an in-flow gradient along the flow direction (Figure 1c). In such a setup, flow forces carry the cells toward the up-gradient regions containing high concentrations of the stressor (Figure 1c, Y). This allows the use of non-motile strains and counteracts a possible evasion of the high stress areas by chemotaxis. In order to realize such an in-flow gradient, the novel miniaturized ALE chip was designed based on a stepwise cumulative increase in concentration of stressors throughout connected compartments (Figure 2a). A hypothetical stress gradient as shown in Figure 2a is achieved by injecting the stressor-free medium into the main inlet while the five side inlets serve to establish a customizable spatial concentration gradient in the subsequent wells by supplying medium with defined stressor concentration and flow rates. The chip comprises six wells (for the dimensions see Figure S1a, Supporting Information), designated as 0, I, II, III, IV, and V, which are connected through passive diffusion mixers (Figure 2b). When the gradient is stabilized under constant flow, a bacterial inoculum can be seeded into the stressor-free well (0) and all resulting progeny cells can be flushed out continuously by flow forces toward the higher stressor levels in the downstream wells I–V. As a result, all cells produced by the biomass in the wells are exposed to the higher stress levels in all subsequent wells. Since only clones with higher fitness will survive, a new population can reside in the wells and grow at the respective stressor level whereas all other clones are washed-out to the waste. Furthermore, the 3D architecture of the wells features a microenvironment with reduced flow velocities at the bottom of the wells to mimic natural niches and enabling the growth

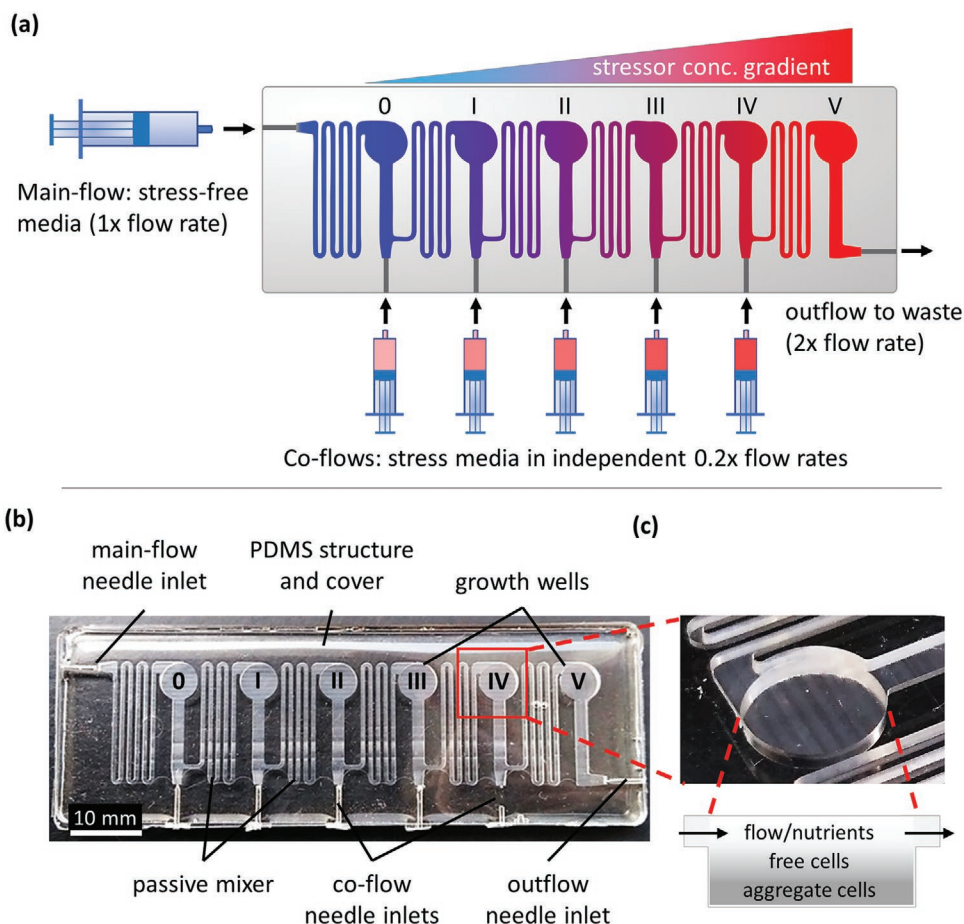


Figure 2. Gradient generation inside the chip and 3D architecture. a) The chemical gradient is cumulatively formed inside the connected wells by gradual supplementation of the main-flow via stepwise addition of defined stressor concentrations at defined flow rates. b) The final chip is made of PDMS and designed to host microbial cultures in wells (c), which can build mixed populations ranging from individual cells, to cell aggregates and biofilms. Well dimensions: $d = 5 \text{ mm}$, $h = 1.2 \text{ mm}$, $v = 23.5 \text{ }\mu\text{L}$. The inset illustrates that wells are 0.7 mm deeper than the channels (height 0.5 mm). For technical details, see Figure S1a, Supporting Information, for the whole chip and Figure S1b, Supporting Information, for the wells.

of biofilms and cell aggregates along with the individual cells on top (Figure 2c).

2.2. Testing and Validation

The constant improvement of microfabrication has led to very sophisticated microfluidic structures, enabling new ways to cultivate, manipulate, and investigate microorganisms down to the single cell level under defined growth conditions.^[38–41] However, such sophisticated systems typically involve complex structures that are difficult to fabricate or operate by non-expert users. Here, we aimed for a simple fabrication method that requires a minimum of microfabrication knowledge and equipment, resulting in a disposable chip. Therefore, we first manufactured a negative structure of the microfluidic chip by milling of a poly(methyl methacrylate) (PMMA) mold, which was then casted as a positive structure using the biocompatible and gas-permeable material polydimethylsiloxane (PDMS) (Figure 2b).

Figure S2, Supporting Information, shows a typical flow setup demonstrating that more than one chip can be run in parallel. In order to validate the chip's ability to create gradients

as designed, the blue dye xylene cyanol FF (XC, $538.61 \text{ g mol}^{-1}$) was utilized to generate a gradient. The XC gradient in the chip was initially simulated using the COMSOL Multiphysics software considering $10 \text{ }\mu\text{L min}^{-1}$ main-flow of water in the main inlet and $2 \text{ }\mu\text{L min}^{-1}$ co-flows with 40 mg L^{-1} of XC in each of the five side inlets (Figure 3a). The same concentrations and flow rates were also experimentally verified employing the full setup comprising the chip and the respective flows (Figure 3b). Both theoretical and experimental analyses showed an identical, uniform XC concentration profile starting from 0 mg L^{-1} in the first well (0) to 20 mg L^{-1} in the last well (V).

For additional confirmation, all six wells were sampled and analyzed spectrophotometrically for their XC concentrations, which confirmed the match between theory and experiment (Figure 3c). Additionally, simulations using other small-molecule substances with different molecular weights, namely ethanol (46.1 g mol^{-1}) and the antibiotic ciprofloxacin (331.3 g mol^{-1}), confirmed that homogenous gradients inside the chip were formed in all cases (Figure S3, Supporting Information).

We then validated the chip's utility for culturing cells and the effects of the chemical gradient on cell survival. To this end, the

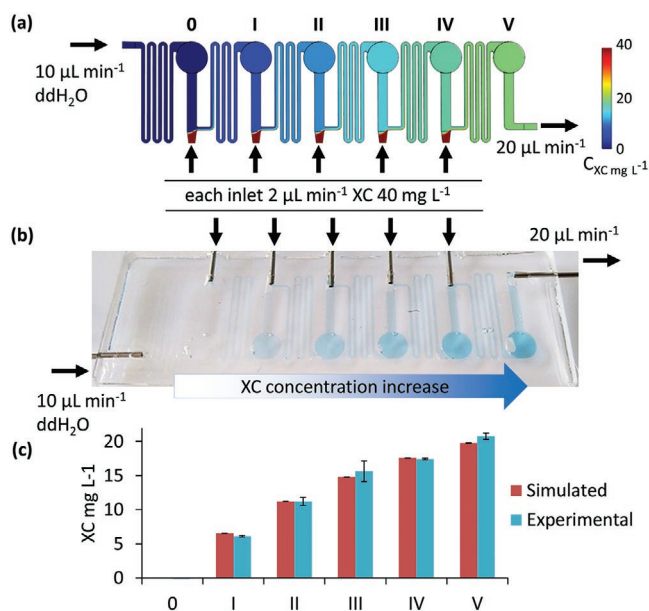


Figure 3. Chemical gradient formation and validation on chip. The chip's functionality for gradient formation was validated by a) simulation and b) experiment using the blue dye xylene cyanol (XC) with the same parameters. c) The concentrations verified experimentally by spectroscopic determination of samples from the individual wells match well with the concentrations derived from simulation. Error bars are SD of five independent determinations in simulated and duplicate measurements in experimental gradients.

model bacterium *Escherichia coli* K12 was cultured in conventional Luria–Bertani (LB) medium, which was used as the source for nutrients as well as a solvent for the stressor substances. In order to establish a proof of concept, an EtOH gradient in LB ranging from 0% to 7% v/v was generated. In this context, the design of our system also allows the use of two sequentially connected chips to ensure a fine resolution of the gradient (Figure S4, Supporting Information). We found that the bacterial growth was impaired at 5.3% EtOH v/v (Figure S4a, Supporting Information, well VI) which is in line with the inhibitory concentration of 5% EtOH v/v, as determined by standard microtiter plate cultivation (Figure S4b, Supporting Information). In this way, precise gradients of chemical stressors can be generated inside the chip, which can be used as a necessary selection pressure for ALE. Notably, air bubbles occasionally accumulated in the wells, but no significant effect on gradient generation was observed, as evidenced by growth inhibition in the corresponding inhibition wells (Figure S4, Supporting Information). This can be attributed to the design of the chip, where the gradient generation is realized via supply of different liquids through the main media and stressors inlets, which are controlled precisely, continuously, and independently by external pumps, and thus are not affected by internal air bubbles in the chip.

Apart from a pronounced stressor concentration in the wells, it is important that the chip design allows potential mutants to have sufficient residence time in the wells to allow for their growth and selection. The chip is operated at an overall flow rate of 20 $\mu\text{L min}^{-1}$ to ensure sufficient nutrient supply to the cells. If only single, planktonic cells were considered, which are pumped through the channel parts of

the chip ($\approx 240 \mu\text{L}$ volume), a theoretical residence time of 12 min would result. At this flow rate, the typical residence time inside a well is 1.3 ± 0.8 min as determined from experiments with *E. coli* being pumped through wells overgrown with biomass (for details see Figure S5, Supporting Information). Hence, total residence times for cells pumped through the chip are substantially lower than the typical *E. coli* division time of 20 min.^[42] This means that all planktonic cells would be quickly flushed out of the chip before they can divide, evolutionary adaptation is unlikely. Therefore, the 3D architecture of the chip was designed in such a way that the bottom of the wells is 0.7 mm below the medium flow from the flow channel (see Figure 2c and Figure S1a, Supporting Information), so that the cells can descend into these lower parts of the well (Figure S1b, Supporting Information) and grow there for longer periods of time as planktonic cells or as non-planktonic cell aggregates. The functionality of this concept is clearly confirmed by the occurrence of turbidity in the wells, ≈ 2 h after inoculation, due to growing biomass (Video S1, Supporting Information). After about 10 h, a quasi-static biomass has established itself in these microenvironments and the residence time of the cells in this biofilm state is variable depending on their position within the well.

In this regard, it is important to note that initial growth started in specific regions of the wells and not in the channels (Figure 4a). This phenomenon can be explained by taking into account simulations of the flow velocities within the chip (Figure 4b). Although the chips are operated at a constant, high flow rate of 20 $\mu\text{L min}^{-1}$, the simulation revealed an inhomogeneous distribution of the velocity in the wells. Flow velocities of up to $25 \times 10^{-4} \text{ m s}^{-1}$ (148 mm min^{-1}) and $1.8 \times 10^{-4} \text{ m s}^{-1}$ (7 mm min^{-1}), respectively, can be observed in the channels and defined areas of the 3D wells (Figure 4b, white arrow), which should lead to an extensive washout of cells. However, near the walls and the bottom of the wells flow velocities of less than $0.12 \times 10^{-4} \text{ m s}^{-1}$ (0.7 mm min^{-1}) occur (Figure 4b, black arrow), enabling cells to remain in the wells for prolonged times (cells will take at least 13 min to traverse a well near the bottom). Notably, over time the profiles of the biomass grown in the chip typically showed a pattern that corresponded to these flow velocity profiles (Figure 4c). It was also observed that high densities of biomass are usually accumulated in areas with low flow velocities (Figure 4b,c, black arrow) while less dense biomass was formed in high velocity areas in the wells (Figure 4b,c, white arrow). These observations confirm that even when using high flows rates to ensure excess of nutrients, the biomass residing in the wells is continuously producing new cells to be transported by flow to the adjacent wells.

The design of the individual wells (see Figure 2c) enables the formation of complex microbial populations in the resulting microenvironments. Individual cells and cell aggregates can detach from the population and are thus moved to the subsequent compartments due to the flow. In contrast, cells in biofilm states reside within the wells for prolonged time. The occurrence of such diverse microbial lifestyles can be examined by optical and microscopic analyses. In order to get an assessment of the resulting population composition inside the chip, *E. coli* was cultivated within the chip for 8 days (Figure 5a(I)). For subsequent analysis, the biomass

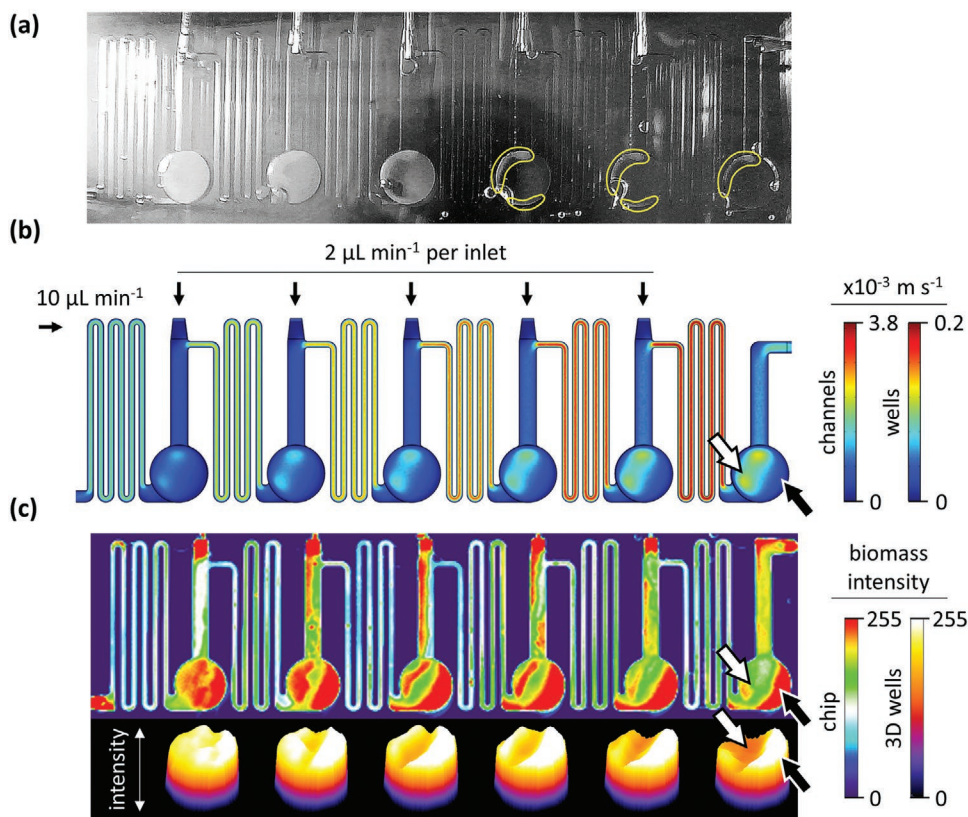


Figure 4. Influence of the flow profile on biomass growth pattern. a) Upon inoculation, the bacterial growth is always initiated in the wells (marked yellow), not in the channels. b) This corresponds well with the simulation of velocity profiles inside the chip using the COMSOL Multiphysics software, demonstrating non-homogeneous velocities in the wells, with high and low velocities indicated by white and black arrows, respectively. Please note that the flow velocities inside the wells are more than a factor of 25 lower than in the channels. c) The *E. coli* biomass distribution can be visualized by imaging and represented in 3D, indicating that the intensity patterns generally follow the flow velocity profile with high biomass intensities being present in low velocity areas (black arrow), and low biomass in high velocity areas (white arrow). The biomass was measured by trans-UV imaging and the intensity maps were calculated using the ImageJ software.

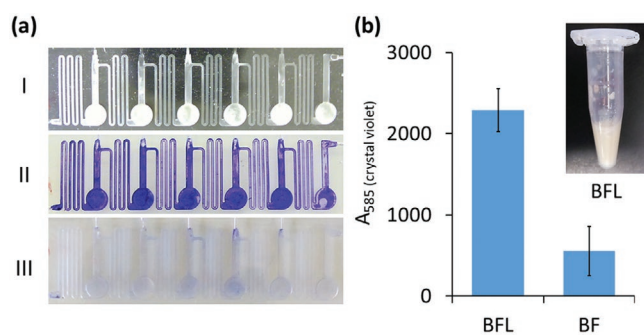


Figure 5. Composition of *E. coli* cultures in the chip. *E. coli* cells were cultivated in chips for 8 days. a) The mature culture inside the chip comprised a biofilm-like (BFL) material (I) which was flushed out using air, collected and quantified using crystal violet (CV) staining. A biofilm (BF) biomass remained attached to the chip surface (II) and could also be stained by CV. The BF was subsequently removed using 33% v/v acetic acid leaving the chip empty (III). b) The total BF and BFL biomass were directly compared using the colorimetric CV assay, which correlates biomass to the absorption at 585 nm. Inset: The BFL material removed from the chip in (I) is intensely opaque and viscous. For a microscopic analysis see Figure S6, Supporting Information. Error bars are the standard deviation (SD) of four samples derived from two independent chip replicas.

was flushed from the chip using air. This material, dubbed biofilm-like (BFL) culture, was found to be of high density, opaque transparency and contained viscous agglomerates of biomass (Figure 5b, Inset). Such BFL material^[43,44] is formed in the wells where it is shielded from the flow shear forces. It consists of a mix of individual cells and cell aggregates in extracellular polymeric substances^[45] leading to biofilm-like structures (Figure S6, Supporting Information). The microscopic analysis of the cell populations within the chip clearly indicated that the chip enabled growth of *E. coli* as individual cells as well as in biofilm and BFL aggregates and that the three forms have a distinctly different morphological appearance (Figure S6, Supporting Information). For quantification, the isolated BFL material as well as the remaining surface-attached biofilm (BF, Figure 5a(II)) were stained with crystal violet (CV).^[46] The residing biofilm was then removed from the chip using 33% acetic acid (Figure 5a(III)) and both BFL and BF samples were quantified by spectrophotometry (Figure 5c). This relative comparison showed that the typical residing BF fraction on average accounts for about $20 \pm 10\%$ of the total biomass in the chip. These results confirm that the chip enables the growth of complex microbial populations under defined stressor concentrations as intended.

2.3. ALE on Chip

The spread of antibiotic resistance is a threatening global issue.^[19,27] One common mechanism bacteria use to quickly evolve resistance is by mutating the DNA encoding for the antibiotic target protein.^[19,47] Since such processes represent a perfect test case for ALE, we employed our chip to evolve resistance to the antibiotics rifampicin (Rif) in *E. coli*. In order to establish gradients, which can efficiently suppress growth of wild type (WT) cells at the higher concentration level, we first determined the concentration-dependent effect of Rif on the growth of *E. coli* in LB using conventional microtiter plate cultivation (Figure S7, Supporting Information). Within the tested range, Rif could affect *E. coli* growth starting at $2.5 \mu\text{g mL}^{-1}$. Significant inhibition was observed at $16 \mu\text{g mL}^{-1}$ and higher, when a large inoculum size of $\text{OD}_{600} 0.2$ was used to replicate the dense starting population to be used in the chip experiments. We then applied Rif in a concentration range of $0\text{--}100 \mu\text{g mL}^{-1}$ to the chip. Importantly, due to the novel design of the chip, different predefined concentrations can be generated in the connected wells to investigate whether population evolvability can be influenced by the spatial gradient profile. Therefore, we defined two different concentration profiles in two independent chips (Figure 6a).

In the first case (chip-A, Figure 6) we replicated the concentrations from the microtiter plate experiment to generate a smooth gradient ranging from no Rif (well 0) to $100 \mu\text{g mL}^{-1}$ Rif (well V). In the second case (chip-B, Figure 6), a steep jump from no Rif in well 0 directly to $100 \mu\text{g mL}^{-1}$ Rif in all other wells (I–V) was generated. Both chips were inoculated in the Rif-free well 0 using an identical *E. coli* K12 monoclonal culture

and then incubated under continuous flow for 6 days to reach the full growth saturation and to verify the chip's ability to perform long-term cultivation (Figure S8a,c and Video S2, Supporting Information). It should be noted that, although the chips were heavily covered with biomass at later stages of the experiment, no clogging of individual wells was observed, even for long cultivation periods of up to 14 days (data not shown). In both chips, growth could be visually observed in the Rif-free wells (0) ≈ 2 h after inoculation (see Video S2, Supporting Information) and substantial growth at the end of the experiment in the wells containing $100 \mu\text{g mL}^{-1}$ Rif in both chips, clearly indicated that the cells had adapted to the presence of rifampicin (Figure 6b). Interestingly, the occurrence of observable growth in the consecutive wells was correlated with the steepness of the gradient (Video S2 and Figure S9, Supporting Information). In chip-A (smooth gradient) growth up to until well III ($16 \mu\text{g mL}^{-1}$ Rif) was already observed after 3.4 h and the cells needed 6.4 h in total to establish growth in well V ($100 \mu\text{g mL}^{-1}$ Rif). At the same concentration in chip-B (well I) growth was observed after approximately the same time, however it took in total more than 16 h to settle in all wells. This nearly parallel growth initiation at $100 \mu\text{g mL}^{-1}$ Rif in both setups suggested that the gradient profile had no significant impact on the evolution. However, subsequent studies on the antibiotic resistance evolved in the two chips showed that this conclusion was not correct. We isolated cells from the individual wells and tested whether they could grow on selective LB agar plates with $100 \mu\text{g mL}^{-1}$ Rif (Figure 6c; Figure S8b,d, Supporting Information). Surprisingly, we found that cells isolated from the smooth gradient profile (chip-A) showed no rifampicin resistant clones

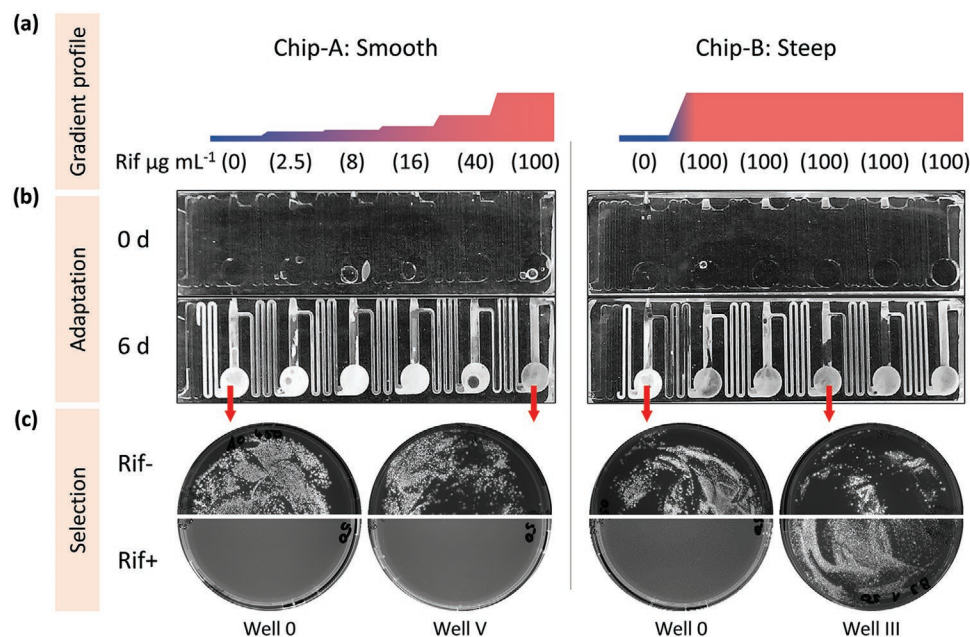


Figure 6. Evolution of rifampicin (Rif) resistance in the chip reveals the critical influence of the gradient profile on *E. coli* adaptability. a) Two concentration profiles were set as a smooth (chip-A) or steep (chip-B) gradients that reach the same final concentration of $100 \mu\text{g mL}^{-1}$ Rif. b) While both gradients showed identical endpoint growth in the chip after 6 days, c) testing of the adapted populations on selective Rif+ agar plates showed the successful evolution of Rif resistance only for cells obtained from the steep gradient chip (plate H). Note that controls plated on the Rif- plates (Figure 6c and Figure S8b, Supporting Information) indicate the presence of living *E. coli* cells in all samples. For daily images and all well data see Figure S8, Supporting Information.

on the selective Rif⁺ plates (Figure 6c; Figure S8b, Supporting Information). In contrast, cells derived from the steep gradient chip-B indeed indicated the evolution of rifampicin resistant clones (Figure 6c well III in chip-B and Figure S8d, Supporting Information). Fivefold repetition of these experiments employing smooth/steep Rif gradient chips confirmed these results. Resistant clones were obtained from steep gradient cultivation (chip-B) in four trials resulting in hundreds of clones per plate (see plate well III in chip-B, in Figure 6c and Figure S8d, Supporting Information), indicating a high incidence of mutations. The smooth gradient (chip-A), however, resulted in resistant clones in only two trials and also in a much lower occurrence of individual resistant clones.

This highly interesting result can be explained by the effects of non-killing doses of antibiotics, which are known to induce bacterial stress responses.^[48] In the smooth gradient chip, the bacterial cells experience sub-inhibitory Rif concentrations in the initial wells, I and II (for rifampicin concentration-dependent growth see Figure S7, Supporting Information). Under these conditions, either the generation of persister cells as well as the formation of a biofilm can be triggered, which can shield the population against antibiotics and thus lead to collaborative protection, also known as persistence.^[49] Or else, stress-induced mutagenesis can occur, which is a hyper mutagenesis mechanism that can result in true genetic resistance.^[50] While “persistence” reflects a transient and restricted phenotypic fitness under certain environmental conditions, “resistance”, on the other hand, is a fixed genotypic adaptation.

Our results indicate that the smooth gradient chip favors the generation of a population of persistent cells, whereas the steep gradient leads to true genetic variation. Triggered by the sub-inhibitory concentration in the initial wells, the phenotypic adaptations might then proliferate to tolerate the more toxic environments in the subsequent wells. However, it has been reported that such persistent cells can eventually evolve into resistant cells.^[47] This scenario in fact explains the rare occurrence of resistant cells observed for the smooth gradient. In contrast, in the steep gradient mode of chip-B, the cells are immediately exposed to Rif levels beyond the inhibitory concentration. The latter situation is known as adapt-or-die,^[28] therefore, only cells that develop appropriate mutations for Rif resistance will survive, migrate to higher wells, and propagate on selective Rif⁺ plates. For a graphical representation of the two processes, see also, Figure S10, Supporting Information.

The importance of the steepness of the gradient is further highlighted, when taking into consideration a different system for adaptation to the antibiotic ciprofloxacin reported by Zhang et al.^[27] In their microarray chip experiments, motile cells were moving toward the areas of highest concentration of ciprofloxacin (so called Goldilocks). Resistant *E. coli* mutants emerged in only 5 h after inoculation with 10⁶ cells.^[27] The authors argue that since WT cells cannot survive under the conditions at the Goldilocks, they are only present at low population densities and posing no competition to the de novo resistant mutants, which can fix rapidly because of their increased fitness to high antibiotic concentrations.^[27,51] Although both systems cannot be directly compared, our results presented here suggest that the WT cell number might not be the key factor in this process.

While we used a comparable initial inoculum in well 0 ($\approx 2.4 \times 10^6$ cells), the accumulation of biomass leads to population sizes of $>10^7$ cells per well, as determined by counting colonies formed by samples from individual wells. This biomass in one well offer a continuous supply of cells to the subsequent wells (see chip-B Video S2, Supporting Information), resulting in a large number of WT cells to potentially compete with the de novo resistant mutants in the selective wells. Still in the steep gradient, we found a high number of mutants (Figure 6c, Rif⁺ in chip-B), correlating with the fact that the Goldilocks structures are also the points of the steepest increase in concentration in the earlier study.^[27] This suggests, that the steepness of the stress gradient is the decisive factor leading to rapid adaptation via stress-induced mutagenesis as also suggested by Frisch and Rosenberg,^[51] and Zhang et al.^[37]

Having successfully established ALE to confer Rif resistance in *E. coli*, we investigated whether the chip can as well be used to generate resistance to other antibiotics with different inhibitory mechanisms. Rifampicin primarily binds to the bacterial DNA-dependent RNA polymerase (RNAP) and impairs the RNA transcription process, which can be prevented by mutations in the *rpoB* gene coding for the RNAP β -subunit.^[52] As a next target we chose nalidixic acid (NA), which binds to the bacterial DNA gyrase thereby interrupting the process of DNA replication.^[53] In this case, resistance is conferred by mutations in genes coding for the DNA gyrase (*gyrAB*) as well as the topoisomerase IV (*parCE*).^[53]

We initially established that growth of *E. coli* was effectively prohibited for NA concentrations greater than 4 $\mu\text{g mL}^{-1}$ (Figure S11a, Supporting Information). We then used a smooth concentration gradient (chip-A) as well as a steep gradient (chip-B), both of which ranged from 0 to 40 $\mu\text{g mL}^{-1}$ NA (Figure S11b, Supporting Information). Again, the cultivation was started by inoculation of *E. coli* in the NA-free well and continued for 6 days (Video S3, Figures S11c and S12a,c, Supporting Information). Analysis was achieved by sampling and plating on selective LB agar plates containing 40 $\mu\text{g mL}^{-1}$ NA. Similar as in the case of Rif, only the steep gradient efficiently produced *E. coli* mutants, which were capable of growing at inhibitory concentrations of NA. In contrast, the smooth gradient yielded no such mutants (Figures S11d and S12b,d, Supporting Information).

To further investigate the acquired mutations, ten randomly selected clones from both the Rif and NA experiments were cultivated in LB broth for 24 h that contained the respective antibiotics and the resulting optical density was determined. Whereas WT *E. coli* revealed an impaired growth, all mutants showed only small variations in the presence or absence of Rif (Figure 7a) and NA (Figure 7b), indicating their high fitness in the presence of antibiotic stress. To further confirm the presence of specific mutations, we analyzed the *rpoB* gene coding for the RNAP β -subunit in case of Rif, and the *gyrA* and *gyrB* genes encoding for the DNA gyrase as well as the *parC* and *parE* genes for the topoisomerase IV in case of NA. These genetic analyses were conducted for five of the adapted mutants randomly selected from both antibiotic adaptations and compared to the WT strain. As expected, relevant mutations were found in the respective genes of all mutants (Figure 7c), while mutations were absent in the parental WT strain.

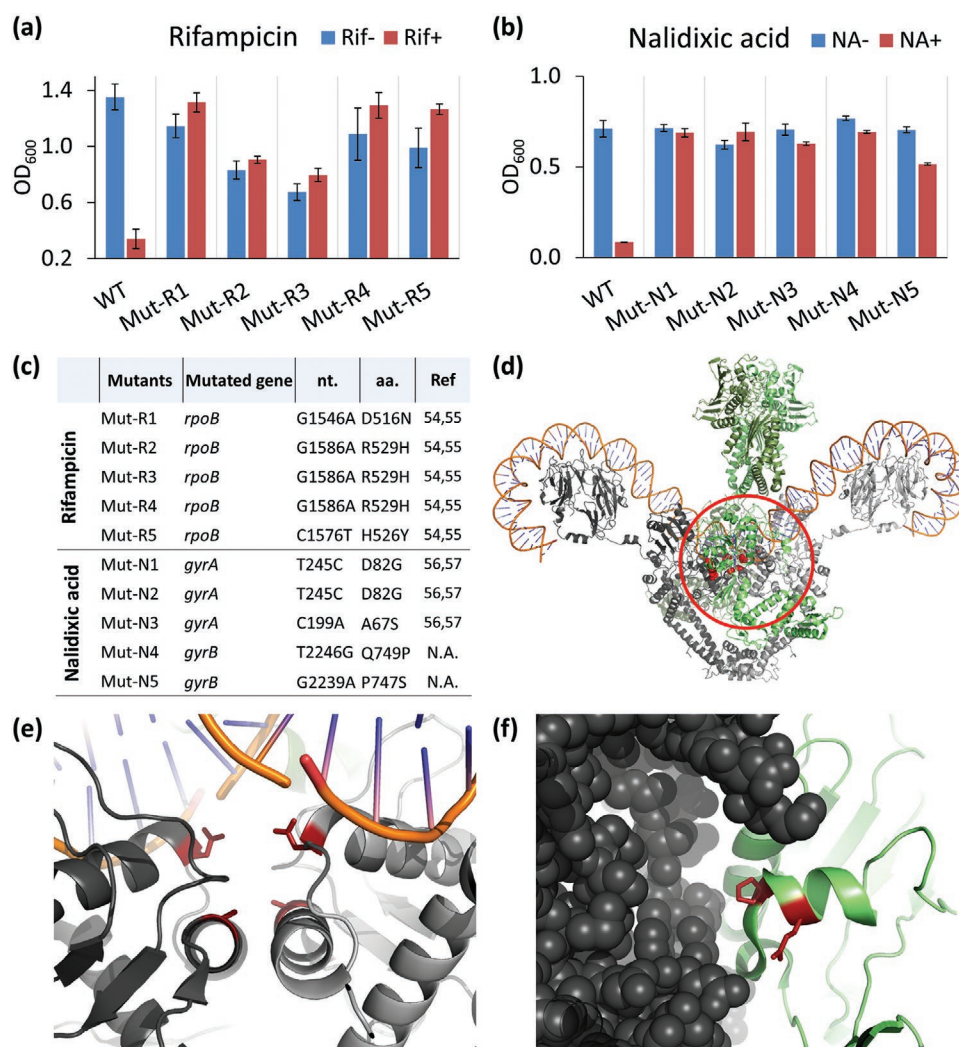


Figure 7. Phenotypic and genotypic validation of *E. coli* mutants adapted to Rif and NA. While the growth of the wild-type *E. coli* for 24 h is impaired by the presence of Rif or NA, randomly selected mutants from the adaptation experiments to a) Rif and b) NA can grow in selective liquid cultures supplemented with 100 $\mu\text{g mL}^{-1}$ of Rif and 40 $\mu\text{g mL}^{-1}$ of NA, respectively. c) Point mutations identified in clones of the adapted *E. coli* mutants in the resistance-conferring genes: *rpoB* for Rif and *gyrA* and *gyrB* for NA. nt. = position of nucleotide in the gene in relation to the *E. coli* K12 genome (GenBank: U00096.3). aa. = position of amino acid in the corresponding protein sequence. d) Molecular structure of the *E. coli* gyrase (PDB ID 6RKW).^[58] Two subunits of GyrA (in gray) and two subunits GyrB (in green) form a complex with a DNA molecule. The resistance conferring mutations in the core of the DNA-enzyme complex (red circle) are shown as the wild-type amino acids depicted in red. e) Two NA-resistance mutations (A67S and D82G) are located at the interface of the DNA and two subunits of gyrase A (dark gray). f) Two previously unknown mutations (P747S and Q749P) are located in a loop of gyrase B (green) facing the surface of the neighboring subunit of gyrase A (dark gray, atoms depicted as spheres). All protein structures were generated based on the available crystal structure data (PDB ID 6RKW)^[58] using the software PyMOL.

All Rif-resistance conferring mutations identified (D516N, H526Y and R529H) as well as two NA-resistance mutations (A67S and D82G) had already been reported in earlier studies^[54–57] and can also be mapped to the respective protein structure (Figure S13, Supporting Information and Figure 7d,e). However, to the best of our knowledge, the two mutations identified in *gyrB* have not previously been described to confer resistance to NA in *E. coli*. Based on the recently published full structure of the complete *E. coli* gyrase,^[58] we could locate the position of our newly identified mutations P747S and Q749P in a loop of the gyrase B subunit, which is facing a neighboring gyrase A subunit (Figure 7f). The newly identified mutations will help to enhance our understanding of the structural basis

for nalidixic acid resistance. Overall, these results clearly emphasize the utility of our chip to trigger diverse, and potentially previously unknown mutations that cause antibiotic resistance. In order to elucidate how the occurrence of mutations within the bacterial population is influenced within the chip, further investigations should focus on the individual contribution of the spatial organization.^[59,60] How the different microbial life forms affect adaptation, especially with respect to yet underexplored lifestyles beyond planktonic and typical surface-attached biofilm states, such as the BFL material, also requires further analysis.^[61] Novel microfluidic devices in combination with appropriate analytical methods can enable the analysis of such mixed populations and co-microbial cultures and improve

the understanding of the molecular basis for their behavior and adaptation.^[41]

3. Conclusion

We here described a novel microfluidic chip that generates tunable and stable spatial concentration gradients in connected compartments, to enable miniaturized ALE procedures. The chip's capability to stably maintain chemical gradients in serial and parallel setups was employed to rapidly evolve *E. coli* resistance to the antibiotics rifampicin and nalidixic acid. The chips' design enables the application of different concentration gradients, which revealed the critical influence of the gradient profile on the adaptability of *E. coli* based on either phenotypic persistence or genetic resistance. Importantly, the microenvironments within the chip create mixed populations ranging from individual cells over biofilm-like cell aggregates to quasi-static biofilms. The combination of these lifestyles within the chip recreates natural conditions better than it is possible with existing ALE methods, which employ planktonic cell cultures. This feature is particularly relevant considering the importance of such mixed populations for evolution.^[16,62] In addition to applications in basic research on complex evolutionary mechanisms, our chip design can also be used for investigations in the biomedical context, such as to understand the development of antibiotic as well as cancer drug resistance.^[63] In combination with automated liquid handling, machine-assisted culturing and analysis^[24] as well as high-throughput genomics and transcriptomics,^[64] the here described ALE chip could also enable miniaturized, highly parallel and cost-effective approaches which could significantly improve the throughput of microbiological experiments such as described here.

4. Experimental Section

Chip Design and Fabrication: The chip consisted of two parts, the structured geometry (76 × 26 mm, 2.5 mm thick) and a flat cover (76 × 26 mm, 0.75 mm thick). The chip's geometry as well as the cover were first designed using the computer aided-design (CAD) software Inventor Professional 2015 (Autodesk Inc., USA), then fabricated as a mold on an 8 mm-thick PMMA, (Evonik Industries) block using micro-milling (Mini Mill GX, Minitech Machinery, US).^[65] The milling program and code was constructed by the software Inventor HSM Pro (Autodesk Inc., USA). After milling, the PMMA molds were cleaned by pressurized air and washed with distilled water.

For casting the chip, the PDMS silicone elastomer was mixed with the curing agent (Sylgard 184, Dow Corning) in a ratio of 10:1, respectively then degassed in vacuum chamber for 1 h. Afterward, the PDMS was poured into the PMMA mold and cured at 70 °C for 1 h. The solid PDMS structure and cover were peeled off the molds and treated by plasma (Plasma Technology GmbH, Germany) facing with the structured side upward. Subsequently the structure and cover were bonded and then incubated at 100 °C for 30 min leading to the final chip. The chips were sterilized by autoclaving at 121 °C for 20 min and stored for further use.

Gradient Validation: Utilizing the chip's CAD geometry, the flow simulation was performed using the software COMSOL Multiphysics (version 5.2.1.152, COMSOL, Inc., USA) with the parameters stated in Figure 3a and Figure S3, Supporting Information. To retrieve a quantitative data from the simulated gradient, concentrations at five different points in every well were averaged as represented in Figure 3c.

For the experimental validation, a stock solution of 40 mg L⁻¹ xylene cyanol FF (XC, Sigma Aldrich Inc., Germany) in ddH₂O was used to fill five 20 mL syringes (B. Braun Melsungen AG, Germany) as co-flows source. One 100 mL syringe (JMS Co. Ltd., Japan) filled with ddH₂O was used as a main-flow source. The end concentrations in the wells were calculated from the solutions mixing equation (Equation (1)).

$$C_x = (F_m C_m + F_c C_c) / (F_m + F_c) \quad (1)$$

Equation (1): Concentration mixing equation for setting or predicting the gradient profile in the chip. C_x : end concentration in a well X . C_m , F_m : concentration and flow rate (in $\mu\text{L min}^{-1}$) of the advent main-flow, respectively. C_c , F_c : concentration and flow rate (in $\mu\text{L min}^{-1}$) of the advent co-flow, respectively.

Main- and co-flow syringes were then installed in two independent syringe pumps (Nexus 3000, Chemyx Inc., USA). To deliver these fluids into the chip, syringes were connected to the chip through silicon tubes (Compagnie de Saint-Gobain, France) with an inner diameter of 1.6 mm, each tube was connected to a cannula of 0.8 mm outer diameter (B. Braun Melsungen AG, Germany) to be mounted into the chip. After installing all the fluidic connections, pumps were started infusing a main-flow of 10 $\mu\text{L min}^{-1}$ water and co-flows of 2 $\mu\text{L min}^{-1}$ XC into the chip as showed in Figure 3b. After running for 4 h at room temperature, the individual wells were sampled (15 μL) using a 1 mL syringe (B. Braun Melsungen AG, Germany) with a 0.45 mm cannula and their absorbance was analyzed in a Synergy H1 plate reader (BioTek Inc., USA) at 610 nm.

ALE on Chip: The lab model bacterium *E. coli* K12 sub-strain MG1655 DSM 18 039 (DSMZ GmbH, Germany) harboring a kanamycin-selection plasmid (pMK-based backbone, lab stock) was used for all biological experiments. Luria-Bertani (LB) medium supplemented with 50 $\mu\text{g mL}^{-1}$ kanamycin was used for normal cultivation, stressor dilution, ALE experiments, and screening of *E. coli* at 37 °C, unless otherwise indicated. A monoclonal cryostock stored at -80 °C was used to inoculate 5 mL LB medium in 10 mL tube and incubated in 180 rpm shaker at 37 °C until its optical density at 600 nm (OD_{600}) reached ≈ 1.0 . The culture was then diluted with fresh LB to a final OD_{600} of 0.2, which had been used to inoculate the chip. The total sterile ALE setup is depicted in Figure S2, Supporting Information. Two main-flow syringes of 100 mL degassed LB (stress-free) were installed in a syringe pump, while 10 co-flow syringes of 20 mL degassed LB supplemented with the corresponding stressor antibiotic (rifampicin and nalidixic acid, PanReac AppliChem, Germany) were installed in a second syringe pump. The chips were connected to the corresponding syringes (each to a main 100 mL and five 20 mL co-flow syringes) through sterile tubes and cannulas as stated above, and the pumping was conducted for 1 h to stabilize the gradients. Afterward, the stress-free wells (0) were inoculated. Inoculation was conducted by injecting 10 μL culture into well 0 by piercing the chip from the side using a sharp needle ($\varnothing 0.45$ mm, B. Braun AG., Germany) connected to a 1 mL syringe. The media flow was stopped before inoculation to allow the cells to settle, and resumed again after 30 min from inoculation and continued until the termination of the experiment. To terminate the ALE experiment, the cannulas were disconnected from the chip, and its wells were sampled as stated above. 1 μL of each sample was diluted in 10 mL fresh LB, mixed well and plated on non-selective as well as selective LB-agar plates supplemented with respective antibiotics (100 $\mu\text{g mL}^{-1}$ Rif and 40 $\mu\text{g mL}^{-1}$ NA). Plates were then incubated at 37 °C for 24 h and the occurrence of adapted mutants was investigated visually.

Characterization of Mutants: Selected mutants from the selective antibiotic plates as well as the wild-type (WT) strain from non-selective plates were inoculated twice, one time into 5 mL of non-selective LB and the second into LB supplemented with the corresponding antibiotic and incubated overnight at 37 °C and 180 rpm. These pre-cultures of the mutants as well as the WT were then diluted with the same fresh media and cultivated in a 96-microtiter plate in a Synergy H1 plate reader, and their growth was recorded every hour for 24 h.

To analyze the mutants and WT genetically, the resistance-conferring genes were amplified by colony PCR using the primers listed in Table S1, Supporting Information. The correct size of the amplified DNA fragments

was confirmed by 0.8% agarose electrophoresis in $0.5 \times$ TAE buffer. Successful PCRs were purified using the DNA Clean and Concentrator kit (Zymo Research Inc., Germany) following the manufacturer's protocol and their sequences were verified (LGC genomics, Germany). The sequence data analysis and mutations localization were performed using the software Geneious 9.1.8 (Biomatters Ltd.).

Analysis of Biomass Composition: To analyze the composition of the biomass cultivated in the chip, *E. coli* was cultivated in two independent chips for 8 days under a continuous flow of LB-Kan using the same setup as described above (ALE on chip) except that the co-flows contained no stressor. Upon termination of the experiment, the chips were first evacuated from all biofilm-like material by pumping air through the main-inlet and collecting the biomass at the outlet. The harvested BFL biomass was stained with a freshly prepared solution of 0.5% CV in ddH₂O for 25 min at room temperature. The remaining attached biomass was incubated in the chips at 70 °C for 45 min to fix the biofilm (BF) to the chip's walls and channels. Subsequently, a freshly prepared solution of 0.5% crystal violet (CV) in ddH₂O was pumped into the chips and incubated for 25 min at room temperature to stain the biomass. After incubation, the CV staining solution was removed from the chips, and the stained chips were washed with ddH₂O and documented. Finally, the stained BF in the chips was dissolved with a solution of acetic acid 33% v/v in ddH₂O. To assess the BF and BFL dissolved CV content, samples were measured for their absorbance at 585 nm using Take3 plate in the reader Synergy H1 (both from BioTek Inc.). A chip containing only LB was treated with identical procedures as a negative control.

Supporting Information

Supporting Information is available from the Wiley Online Library or from the author.

Acknowledgements

The authors acknowledge financial support of this work by the Helmholtz programme, BioInterfaces in Technology and Medicine (BIFTM). A.E.Z. thanks the German Academic Exchange Service (DAAD) and the Egyptian Ministry of Higher Education (MOHE) for funding his Ph.D. fellowship. The authors thank Simon Reifenschweiler for help on CAD design, fabrication, and COMSOL simulation.

Open access funding enabled and organized by Projekt DEAL.

Conflict of Interest

The authors declare no conflict of interest.

Data Availability Statement

Research data are not shared.

Keywords

adaptive laboratory evolution, antibiotic resistance, biofilms, gradients, lab-on-a-chip, mutations

Received: November 13, 2020

Revised: December 22, 2020

Published online:

[1] J. L. Payne, A. Wagner, *Nat. Rev. Genet.* **2019**, *20*, 24.

[2] M. Dragosits, D. Mattanovich, *Microb. Cell Fact.* **2013**, *12*, 64.

- [3] V. A. Portnoy, D. Bezdan, K. Zengler, *Curr. Opin. Biotechnol.* **2011**, *22*, 590.
- [4] B. Van den Bergh, T. Swings, M. Fauvart, J. Michiels, *Microbiol. Mol. Biol. Rev.* **2018**, *82*, e00008.
- [5] L. J. Jahn, C. Munck, M. M. H. Ellabaan, M. O. A. Sommer, *Front. Microbiol.* **2017**, *8*, 1.
- [6] V. Lázár, G. P. Singh, R. Spohn, I. Nagy, B. Horváth, M. Hrtyan, R. Busa-Fekete, B. Bogos, O. Méhi, B. Csörgő, G. Pósfai, G. Fekete, B. Szappanos, B. Kégl, B. Papp, C. Pál, *Mol. Syst. Biol.* **2013**, *9*, 700.
- [7] M. J. McDonald, *EMBO Rep.* **2019**, *20*, e46992.
- [8] I. Matic, *Period. Biol.* **2017**, *118*, 363.
- [9] V. Mozhayskiy, I. Tagkopoulos, *Integr. Biol.* **2013**, *5*, 262.
- [10] T. Horinouchi, T. Minamoto, S. Suzuki, H. Shimizu, C. Furusawa, *J. Lab. Autom.* **2014**, *19*, 478.
- [11] V. Wallace-Salinas, M. F. Gorwa-Grauslund, *Biotechnol. Biofuels* **2013**, *6*, 151.
- [12] E. de Crécy, D. Metzgar, C. Allen, M. Pénicaud, B. Lyons, C. J. Hansen, V. de Crécy-Lagard, *Appl. Microbiol. Biotechnol.* **2007**, *77*, 489.
- [13] B. G. Wong, C. P. Mancuso, S. Kiriakov, C. J. Bashor, A. S. Khalil, *Nat. Biotechnol.* **2018**, *36*, 614.
- [14] P. S. Stewart, M. J. Franklin, *Nat. Rev. Microbiol.* **2008**, *6*, 199.
- [15] D. O. Serra, R. Hengge, *Environ. Microbiol.* **2014**, *16*, 1455.
- [16] K. Nagy, Á. Ábrahám, J. E. Keymer, P. Galajda, *Front. Microbiol.* **2018**, *9*, 496.
- [17] F. J. H. Hol, B. Hubert, C. Dekker, J. E. Keymer, *ISME J.* **2016**, *10*, 30.
- [18] M. Baym, T. D. Lieberman, E. D. Kelsic, R. Chait, R. Gross, I. Yelin, R. Kishony, *Science* **2016**, *353*, 1147.
- [19] R. Hermsen, J. B. Deris, T. Hwa, *Proc. Natl. Acad. Sci. U. S. A.* **2012**, *109*, 10775.
- [20] W. Zhou, J. Le, Y. Chen, Y. Cai, Z. Hong, Y. Chai, *TrAC, Trends Anal. Chem.* **2019**, *112*, 175.
- [21] O. Scheler, W. Postek, P. Garstecki, *Curr. Opin. Biotechnol.* **2019**, *55*, 60.
- [22] S. M. Bjork, H. N. Joensson, *Curr. Opin. Biotechnol.* **2019**, *55*, 95.
- [23] D. B. Weibel, W. R. DiLuzio, G. M. Whitesides, *Nat. Rev. Microbiol.* **2007**, *5*, 209.
- [24] S. H. Hansen, T. Kabbeck, C. P. Radtke, S. Krause, E. Krolitzki, T. Peschke, J. Gasmi, K. S. Rabe, M. Wagner, H. Horn, J. Hubbuch, J. Gescher, C. M. Niemeyer, *Sci. Rep.* **2019**, *9*, 8933.
- [25] B. Li, Y. Qiu, A. Glidle, D. McIlvenna, Q. Luo, J. Cooper, H.-C. Shi, H. Yin, *Anal. Chem.* **2014**, *86*, 3131.
- [26] S. Kim, S. Lee, J.-K. Kim, H. J. Chung, J. S. Jeon, *Biomicrofluidics* **2019**, *13*, 014108.
- [27] Q. Zhang, G. Lambert, D. Liao, H. Kim, K. Robin, C.-k. Tung, N. Pourmand, R. H. Austin, *Science* **2011**, *333*, 1764.
- [28] J. Deng, L. Zhou, R. A. Sanford, L. A. Shechtman, Y. Dong, R. E. Alcalde, M. Sivaguru, G. A. Fried, C. J. Werth, B. W. Fouke, *Environ. Sci. Technol.* **2019**, *53*, 7996.
- [29] M. DiCicco, S. Neethirajan, *BioChip J.* **2014**, *8*, 282.
- [30] Z. Hou, Y. An, K. Hjort, K. Hjort, L. Sandegren, Z. Wu, *Lab Chip* **2014**, *14*, 3409.
- [31] Z. Liu, H. Sun, K. Ren, *ChemPlusChem* **2017**, *82*, 792.
- [32] J. Diao, L. Young, S. Kim, E. A. Fogarty, S. M. Heilman, P. Zhou, M. L. Shuler, M. Wu, M. P. DeLisa, *Lab Chip* **2006**, *6*, 381.
- [33] R. E. Lenski, *ISME J.* **2017**, *11*, 2181.
- [34] E. Choi, H. Chang, C. Y. Lim, T. Kim, J. Park, *Lab Chip* **2012**, *12*, 3968.
- [35] T. Long, R. M. Ford, *Environ. Sci. Technol.* **2009**, *43*, 1546.
- [36] D. Irimia, D. A. Geba, M. Toner, *Anal. Chem.* **2006**, *78*, 3472.
- [37] Q. Zhang, K. Robin, D. Liao, G. Lambert, R. H. Austin, *Mol. Pharmaceutics* **2011**, *8*, 2063.
- [38] F. J. H. Hol, C. Dekker, *Science* **2014**, *346*, 1251821.
- [39] F. K. Balagadde, *Science* **2005**, *309*, 137.

- [40] J. Mannik, R. Driessen, P. Galajda, J. E. Keymer, C. Dekker, *Proc. Natl. Acad. Sci. U. S. A.* **2009**, *106*, 14861.
- [41] A. Burmeister, A. Grünberger, *Curr. Opin. Biotechnol.* **2020**, *62*, 106.
- [42] G. Sezonov, D. Joseleau-Petit, R. D'Ari, *J. Bacteriol.* **2007**, *189*, 8746.
- [43] M. Alhede, K. N. Kragh, K. Qvortrup, M. Allesen-Holm, M. van Gennip, L. D. Christensen, P. Ø. Jensen, A. K. Nielsen, M. Parsek, D. Wozniak, S. Molin, T. Tolker-Nielsen, N. Høiby, M. Givskov, T. Bjarnsholt, *PLoS One* **2011**, *6*, e27943.
- [44] Y.-G. Jung, J. Choi, S.-K. Kim, J.-H. Lee, S. Kwon, *Appl. Environ. Microbiol.* **2015**, *81*, 211.
- [45] M. Vert, Y. Doi, K.-H. Hellwich, M. Hess, P. Hodge, P. Kubisa, M. Rinaudo, F. Schué, *Pure Appl. Chem.* **2012**, *84*, 377.
- [46] G. A. O'Toole, *J. Visualized Exp.* **2011**, *10*, e2437.
- [47] I. Levin-Reisman, I. Ronin, O. Gefen, I. Braniss, N. Shoshani, N. Q. Balaban, *Science* **2017**, *355*, 826.
- [48] D. I. Andersson, D. Hughes, *Nat. Rev. Microbiol.* **2014**, *12*, 465.
- [49] C. A. Fux, J. W. Costerton, P. S. Stewart, P. Stoodley, *Trends Microbiol.* **2005**, *13*, 34.
- [50] M. A. Kohanski, M. A. DePristo, J. J. Collins, *Mol. Cell* **2010**, *37*, 311.
- [51] R. L. Frisch, S. M. Rosenberg, *Science* **2011**, *333*, 1713.
- [52] D. J. Jin, C. A. Gross, *J. Mol. Biol.* **1988**, *202*, 45.
- [53] K. J. Aldred, R. J. Kerns, N. Osheroff, *Biochemistry* **2014**, *53*, 1565.
- [54] A. H. Badran, D. R. Liu, *Nat. Commun.* **2015**, *6*, 8425.
- [55] L. Garibyan, *DNA Repair* **2003**, *2*, 593.
- [56] D. C. Hooper, *Drug Resist. Updates* **1999**, *2*, 38.
- [57] J. Ruiz, *J. Antimicrob. Chemother.* **2003**, *51*, 1109.
- [58] A. V. Broeck, C. Lotz, J. Ortiz, V. Lamour, *Nat. Commun.* **2019**, *10*, 4935.
- [59] W. Kim, F. Racimo, J. Schluter, S. B. Levy, K. R. Foster, *Proc. Natl. Acad. Sci. U. S. A.* **2014**, *111*, E1639.
- [60] S. Mitri, E. Clarke, K. R. Foster, *ISME J.* **2016**, *10*, 1471.
- [61] A. J. Paula, G. Hwang, H. Koo, *Nat. Commun.* **2020**, *11*, 1354.
- [62] Z. Bódi, Z. Farkas, D. Nevozhay, D. Kalapis, V. Lázár, B. Csörgő, Á. Nyerges, B. Szamecz, G. Fekete, B. Papp, H. Araújo, J. L. Oliveira, G. Moura, M. A. S. Santos, T. Székelyjr., G. Balázs, C. Pál, *PLoS Biol.* **2017**, *15*, e2000644.
- [63] G. Lambert, L. Estévez-Salmeron, S. Oh, D. Liao, B. M. Emerson, T. D. Tlsty, R. H. Austin, *Nat. Rev. Cancer* **2011**, *11*, 375.
- [64] J. A. Reuter, D. V. Spacek, M. P. Snyder, *Mol. Cell* **2015**, *58*, 586.
- [65] M. Grösche, A. E. Zoheir, J. Stegmaier, R. Mikut, D. Mager, J. G. Korvink, K. S. Rabe, C. M. Niemeyer, *Small* **2019**, *15*, 1901956.